Mechanics of dislocation pile-ups: A unification of scaling regimes

L. Scardia[a,b,c,*], R.H.J. Peerlings[b,*], M.A. Peletier[c,d], M.G.D. Geers[b]

[a] *Materials innovation institute (M2i)*
[b] *Department of Mechanical Engineering, Technische Universiteit Eindhoven, The Netherlands*
[c] *Department of Mathematics and Computer Sciences, Technische Universiteit Eindhoven, The Netherlands*
[d] *Institute for Complex Molecular Systems, Technische Universiteit Eindhoven, The Netherlands*

Abstract

This paper unravels the problem of an idealised pile-up of n infinite, equi-spaced walls of edge dislocations at equilibrium. We define a dimensionless parameter that depends on the geometric, constitutive and loading parameters of the problem, and we identify five different scaling regimes corresponding to different values of that parameter for large n. For each of the cases we perform a micro-to-meso upscaling, and we obtain five expressions for the mesoscopic (continuum) internal stress. The upscaling method we illustrate here can be made mathematically rigorous, as we show in the companion paper [13]. The focus of the present paper is on the mechanical interpretation of the resulting internal stresses. In the continuum limit we recover some expressions for the internal stress that are already in use in the mechanical community, as well as some new models. The results in this paper offer a unifying approach to such models, since they can be viewed as the outcome of the same discrete dislocation setup, for different values of the dimensionless parameter (i.e., for different local dislocations arrangements). In addition, the rigorous nature of the upscaling removes the need for ad hoc assumptions.

Keywords: Dislocations, pile-up, internal stress, plasticity.

1. Introduction

Dislocations occupy a central position in discussions of the permanent deformation of metals because of their role as the main carriers of plastic deformation. Therefore it is necessary to incorporate their presence, or the main effect of their presence, in a plasticity model that aims for a predictive power. However, since the typical number of dislocations even in a small sample of the material is very high, formulating a model that keeps track of every single dislocation is out of reach except for very small-scale problems. This explains the interest in describing the collective behaviour of dislocations in terms of a continuum quantity: the dislocation density.

The challenge in this scale transition consists in describing the time evolution of the dislocation density in a physically-driven way, by performing a rigorous upscaling from the dislocation

*Corresponding author. Current affiliation: School of Mathematics and Statistics, University of Glasgow, United Kingdom, tel.: +44 141 3304567

Email addresses: Lucia.Scardia@glasgow.ac.uk (L. Scardia), R.H.J.Peerlings@tue.nl (R.H.J. Peerlings), M.A.Peletier@tue.nl (M.A. Peletier), M.G.D.Geers@tue.nl (M.G.D. Geers)

scale to the dislocation density scale (also called *meso-scale*). This task has been mainly pursued phenomenologically or by means of a statistical mechanics approach and has produced a number of competing models (e.g. [7, 8, 10, 15, 16, 27]). In the case of parallel, straight dislocations, the evolution of the dislocation density $\rho(x,t)$ (here we assume, for simplicity, that all the dislocations have the same Burgers vector) is described in terms of the continuity equation

$$\partial_t \rho + \partial_x(\rho v) = 0,$$

where the velocity v driving the evolution is of the form

$$v = \frac{b}{B}(\sigma - \sigma_{\text{int}}), \tag{1}$$

with b denoting the Burgers vector, B a linear drag coefficient, σ an externally applied shear stress (constant, for simplicity) and $\sigma_{\text{int}} = \sigma_{\text{int}}(x, \rho, \partial_x \rho)$ an internal stress accounting for the net effect of the interactions among dislocations. The different models available in the literature differ in the internal stress expressions that they propose; the range of validity of the proposed theories is typically unclear, as well as the conditions under which one of them is to be preferred over another one. In fact most of the models have been derived phenomenologically, often starting from an *ad hoc* Ansatz, or assumptions have been made in the derivation that are not always justified.

Here comes the essential difference of our approach: The continuum models for the dislocation density we propose can be obtained from a more fundamental discrete dislocation model using a rigorous mathematical approach (Γ-convergence; see [13]). As a consequence, we obtain an exact classification of limiting behaviour for the system that we study, which unifies existing, independently derived descriptions into a coherent framework, and identifies new regimes that have not yet been studied.

In order to rely on the completely justified and rigorous derivation in [13], our starting point has to be an idealised dislocation configuration. More precisely, we consider the discrete model of an idealised pile-up of dislocations studied in [28] (see also [14, 19, 18, 2, 24]). This model describes the equilibrium positions of n dislocation walls under the influence of an applied stress σ that pushes the walls towards an impenetrable barrier; the barrier is modelled as a wall of pinned dislocations at $x_0 = 0$ (see Section 2 for the detailed description). The discrete equilibrium equations for the positions of the n walls can be written in the general form

$$\sigma^i_{\text{int}} - \sigma = 0, \quad i = 1, \dots, n, \tag{2}$$

where the discrete internal stress for the i-th wall is the sum of the contributions due to the interactions with the other walls (see (3) for the detailed expression of the equations). Therefore, in view of (1), the system (2) is nothing but $v_i = 0$, where v_i is the velocity of the i-th wall. At this point one can intuitively imagine that passing to the (continuum) limit in the discrete equation (2) should give a continuum analog of (1) for $v = 0$, and consequently an expression for a continuum version of the internal stress. This is exactly the object we want to characterise.

Our approach is different from the upscaling procedure followed in the quoted papers that considered the same pile-up configuration. In [19, 18] the convergence of stationary states is proved using formal methods, in a special case of our analysis. Moreover, while [2, 24] perform a two-step discrete-to-continuum upscaling by smearing out the dislocations first in the slip plane and then in the in-wall direction, we upscale in the two directions simultaneously. We stress that

the continuum model we derive is in perfect agreement with our starting discrete model (see Figures 7, 8, 9, 12 and 13). We recall that in [2, 24], as the authors point out, the resulting continuum model has to be corrected to incorporate the missing interaction.

An interesting novelty in our result is that the mesoscopic internal stress we obtain does not depend on the dislocation density (and its gradient) only, but it also contains some more *local* information about the discrete arrangement of the dislocations, that the density alone fails to capture. To be more precise, consider the two arrangements in Figure 1. They correspond to the same density, i.e., to the same number of dislocations per unit volume. But the dislocation patterns in the two cases are different and this will result in different expressions for the upscaled internal stress describing the overall interactions in the two cases. This additional *local* information on the arrangement of the dislocations can be expressed in terms of an aspect ratio a, defined as the ratio between the typical distance Δx between two consecutive dislocations in the same row (slip plane) and the distance h between two consecutive dislocations in the same wall. In Figure 1 the first arrangement corresponds to $a = \frac{\Delta x}{h} \sim 1$, the second one to $a = \frac{\Delta x}{h} \ll 1$.

Figure 1: Two different arrangements corresponding to the same density in the rectangle.

The upscaling procedure we adopt for the micro-to-meso upscaling (which is briefly presented here and proved in detail in [13]) is based on Γ-convergence, a variational convergence which is well-known in the mathematical community and has been successfully applied to a variety of problems in materials science, from fracture mechanics to homogenization, from magnetomechanics to dimension reduction, see, e.g. [1, 5, 29]. In particular, it has been recently used to tackle problems in dislocation theory ([11, 12, 26]), although in the quoted papers the focus is on the core energy rather than on interactions.

On the contrary, our approach focuses on the discrete energy of a system of interacting dislocations (the minimisers of the energy are exactly the solutions to (2)). The discrete-to-continuum upscaling is done by letting the number of dislocations n become infinitely large. Note that this is not the same as having infinite dislocation density, since we also rescale the dislocation density. This can be thought of as *zooming out* from the micro-scale to the continuum scale. According to the different asymptotic behaviour of the aspect ratio a (i.e., according to the *local* distribution of the dislocations), five different expressions for the continuum energy can be derived (we refer to [13] for the details of the mathematical procedure); and, accordingly, five different expressions for the upscaled internal stress.

The results we obtain show that the simplified discrete model taken as a starting point is not *too simple*: the internal stresses resulting from our derivation are more general than many well-known models proposed in the engineering literature (see [9, 10, 16]). More precisely, our result contains as a special case the internal stresses proposed in the quoted papers, explaining their range of validity. The comparison with previous models will be the subject of Section 5.

The key advantage of our rigorous approach to upscaling is that it is exact. This means

that once a discrete model is chosen (with its simplifications and limitations) the corresponding upscaled continuum model obtained by following our method is uniquely determined. Moreover, the fact that no simplifying assumptions are made in the derivation (but only at the level of the discrete model) explains why such a rich variety of continuum models can be obtained, even from a relatively simple model. This is not the case for other upscaling methods, where the starting point can be more general, but a number of restrictions and simplifications are typically made in the derivation, affecting the generality of the upscaled models and their range of validity.

The plan of the paper is as follows. In Section 2 we state the discrete problem and comment on our special choice for the arrangement of the dislocations. An overview of the methods and of the results is given in Section 3, while the upscaling is considered in Sections 4. A comparison between our results and other well-known models in the engineering literature is the subject of Section 5, together with a number of other comments.

2. Statement of the problem

The problem we are considering is the equilibrium of a system of n walls of straight edge dislocations (all with the same Burgers vector $\mathbf{b} = b\mathbf{e_1}$) under the action of an externally applied shear stress that pushes the walls towards an impenetrable barrier.

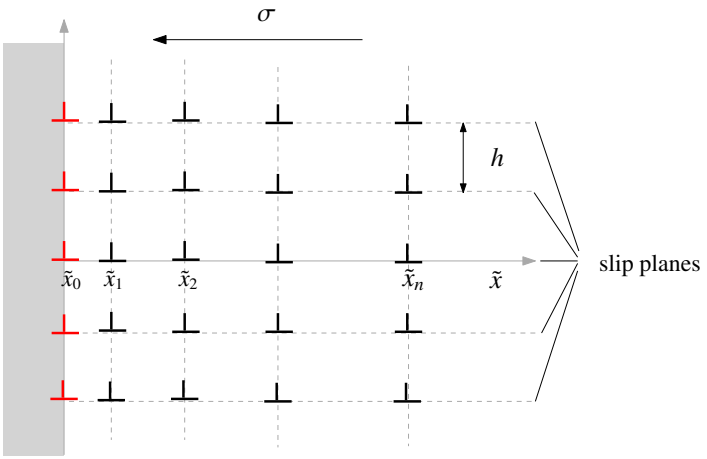

Figure 2: Pile-up of discrete dislocation walls. The walls are at positions $\tilde{x}_i > 0$ and the barrier is modelled as a wall of pinned dislocations at $\tilde{x} = \tilde{x}_0 = 0$.

Consecutive dislocations within the same wall are assumed to be equidistant, at distance $h > 0$, and we assume there are infinitely many dislocations in each wall. The impenetrable barrier is modelled as an infinite wall of pinned dislocations (the plane $\tilde{x} = 0$). We moreover assume that the walls are perfectly aligned (see Figure 2). Therefore the model is essentially one-dimensional, the only unknowns being the positions $\tilde{x}_1, \ldots, \tilde{x}_n$ of the n dislocation walls.[1]

[1]From here on, tildes distinguish dimensional quantities from their non-dimensional counterparts; we will define non-dimensional positions x_i below.

While it is common in the literature to reduce to the case of straight dislocations and to consider a single slip system, the assumption of having dislocations arranged in vertical walls is clearly a simplification (even if used in many papers, see e.g. [2, 24, 19, 18, 28, 14]). On the other hand, this idealised configuration allows us to carry out a rigorous analysis, whereas more random configurations would require a statistical approach. Such a statistical approach, however, would typically require some additional assumptions in the derivation, and therefore it might well result in a limit model that is less general than the one rigorously derived from a more idealised setting.

Moreover, although the discrete model we consider is highly idealised, it has a number of properties that make it both interesting and not unrealistic. The fact that multiple dislocations move along exactly the same slip plane is natural, because of the way they are generated from *Frank-Read sources* (e.g. [23, Sec. 8.6]). Also, equispaced vertical walls are minimal-energy configurations. Walls of edge dislocations are locally stable, in the sense that if one of the dislocations deviates from its wall position, either horizontally or vertically, it experiences a restoring force that pushes it back. Finally, the vertical organization in walls is also justified by correlation functions calculated from numerical simulations (e.g. [16]). For these reasons we believe that our simplified discrete system is not too simple and that it is worth exploring. Moreover, the mesoscopic models we obtain are general enough to contain as a special case several well-known models in the engineering literature, including some models derived by statistical arguments.

The equilibrium positions of the dislocation walls are obtained by solving the equations

$$\frac{K}{h}\sum_{\substack{j=0\\ j\neq i}}^{n}\varphi\left(\frac{\tilde{x}_i-\tilde{x}_j}{h}\right)-\sigma=0,\qquad i=1,\dots,n, \tag{3}$$

where $\varphi(s)=\frac{s}{\sinh^2\pi s}$ is the (globally repulsive) stress governing the wall-wall interactions, $-\sigma$ is the constant applied shear stress, and $K:=\frac{\pi Gb}{2(1-\nu)}$, b being the length of the Burgers vector, ν the Poisson's ratio and G the shear modulus. Note that φ is obtained by superimposing the stress generated by every individual dislocation in the wall (i.e., $\sigma_{xy}(x,y)=\frac{x(x^2-y^2)}{(x^2+y^2)^2}$, up to a multiplicative constant), see [22, Sec. 19-5] and [28].

Solving (3) numerically gives a vector $\tilde{x}\in\mathbb{R}^n$; the i-th component of the vector represents the equilibrium position of the i-th dislocation wall. In Figure 3 we plot the discrete dislocation

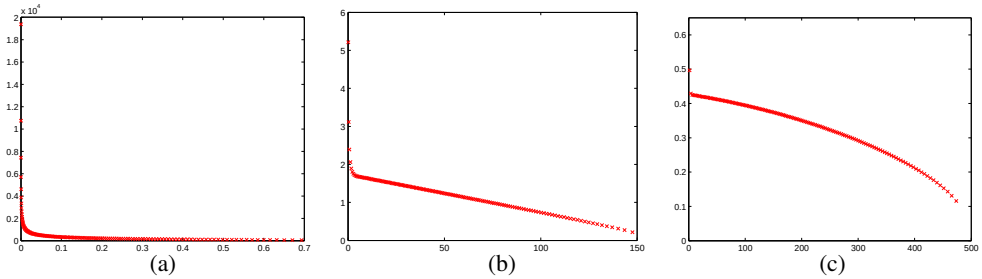

Figure 3: Plots of the discrete dislocation density defined as in (4) corresponding to solutions of (3) for different values of the applied stress σ. In all the plots $K=1$, $n=150$, and $h=10$; in (a) $\sigma=40$; in (b) $\sigma=0.01$; in (c) $\sigma=0.0005$.

density defined in terms of the equilibrium positions as

$$\tilde{\rho}^d(\tilde{x}_i) := \frac{1}{\tilde{x}_i - \tilde{x}_{i-1}}, \qquad i = 1, \dots, n, \tag{4}$$

for different values of the applied stress σ. Note that for large values of σ the pile-up region is small and the dislocation density is very high, while for smaller values of the stress a rather linear behaviour of the density is prominent at first, and then a more rapid decay. This suggests that, depending on the problem parameters, some behaviour of the density is dominant in the bulk (while at the boundary of the pile-up region the occurrence of *boundary layers* is expected).

However, a discrete numerical approach is unfeasible for a large number of dislocation walls, and an average information in terms of a continuum dislocation density should be preferred.

3. Discrete energy formulation, scaling regimes and main result

The first step in our discrete-to-continuum upscaling procedure is to write down the discrete energy whose minimisers satisfy the equilibrium equations (3), by exploiting the variational structure of the equilibrium equations. The upscaling procedure will then be carried out on the discrete energy and will produce a continuum energy functional. The equilibrium equation associated with the upscaled limit functional is exactly the *upscaled* version of the discrete equations and hence characterises the mesoscopic internal stress as desired.

3.1. Discrete dislocation energy and scaling regimes

We define the energy associated to the equations (3). For $\tilde{x} \in \mathbb{R}^n$ let $\tilde{E}_n(\tilde{x})$ be defined as:

$$\tilde{E}_n(\tilde{x}) := \frac{K}{2} \sum_{i=0}^{n} \sum_{\substack{j=0 \\ j \neq i}}^{n} V\left(\frac{\tilde{x}_i - \tilde{x}_j}{h}\right) + \sigma \sum_{i=0}^{n} \tilde{x}_i, \tag{5}$$

where V is the primitive of $-\varphi$ which decays to zero at infinity and is plotted in Figure 4.

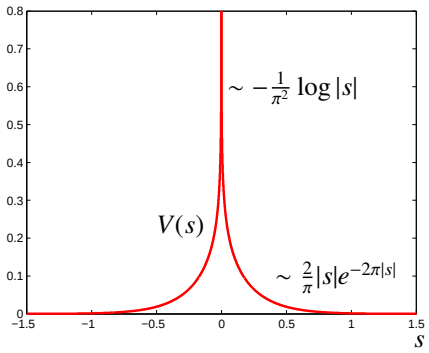

Figure 4: The interaction energy V.

More precisely, V is defined as

$$V(s) := \frac{1}{\pi} s \coth \pi s - \frac{1}{\pi^2} \log(2 \sinh \pi s). \tag{6}$$

Equations (3) are equivalent to $\partial_{\tilde{x}_i}\tilde{E}_n = 0$. Using the fact that $V(s) = V(-s)$ we can rewrite the sum in (5) in a form that will be more convenient for our analysis, as

$$\tilde{E}_n(\tilde{x}) = K\sum_{k=1}^{n}\sum_{j=0}^{n-k} V\left(\frac{\tilde{x}_{j+k}-\tilde{x}_j}{h}\right) + \sigma\sum_{j=0}^{n}\tilde{x}_j. \tag{7}$$

The first term in the energy (7) penalises configurations where the dislocations are close to one another, since the density V blows up logarithmically in zero, while it favours configurations where dislocations are at large distance from one another, since V decays exponentially at infinity. Hence the interaction between two dislocation walls is fully repulsive. The second term of the energy, on the contrary, is a confinement term that penalises configurations where the dislocations are far from the obstacle at $\tilde{x} = 0$.

We convert (7) into a dimensionless form that will be used in the discrete-to-continuum derivation. We first non-dimensionalize the dislocation positions $\tilde{x}_i$ by introducing the new dimensionless variables x_i,

$$x_i := \frac{\tilde{x}_i}{\ell_n},$$

where ℓ_n is a length scale of the same order as the pile-up length. Given ℓ_n, the *aspect ratio* α_n is the ratio between the average dislocation distance $\Delta\tilde{x} \sim \frac{\ell_n}{n}$ and the vertical spacing h between consecutive dislocations in the same wall:

$$\alpha_n := \frac{\ell_n}{nh}.$$

We now rewrite the energy (7) in a dimensionless form, in terms of the new variable x:

$$E_n(x) := \frac{\tilde{E}_n(nh\alpha_n x)}{n^2\sigma h\alpha_n} = \frac{K}{n^2\sigma h\alpha_n}\sum_{k=1}^{n}\sum_{j=0}^{n-k} V\left(n\alpha_n(x_{j+k}-x_j)\right) + \frac{1}{n}\sum_{j=0}^{n} x_j. \tag{8}$$

The aspect ratio α_n is a local description of the average arrangement of the dislocations within the pile-up region. Figure 5 illustrates the possible scalings of α_n and some of the corresponding discrete configurations.

More precisely, we consider the following cases:

(1) Subcritical regime: $\alpha_n \ll \frac{1}{n}$;
(2) First critical regime: $\alpha_n \sim \frac{1}{n}$;

$\Big\}$ $\frac{\ell_n}{h} \lesssim 1$

(3) Intermediate regime: $\frac{1}{n} \ll \alpha_n \ll 1$;
(4) Second critical regime: $\alpha_n \sim 1$;
(5) Supercritical regime: $\alpha_n \ll 1$.

$\Big\}$ $\frac{\ell_n}{h} \gg 1$

3.2. Main result: Continuum dislocation energy

The most convenient concept to connect the discrete (finite n) situation with its infinite-n limit is the discrete dislocation *density* $\rho_n = \frac{1}{n}\sum_{i=1}^{n}\delta_{x_i}$, where δ_{x_i} is the Dirac delta function localised at x_i (and is zero everywhere except at x_i). The measure ρ_n describes the distribution of the walls and is approximately a dimensionless version of the discrete density $\tilde{\rho}^d$ introduced in (4). For

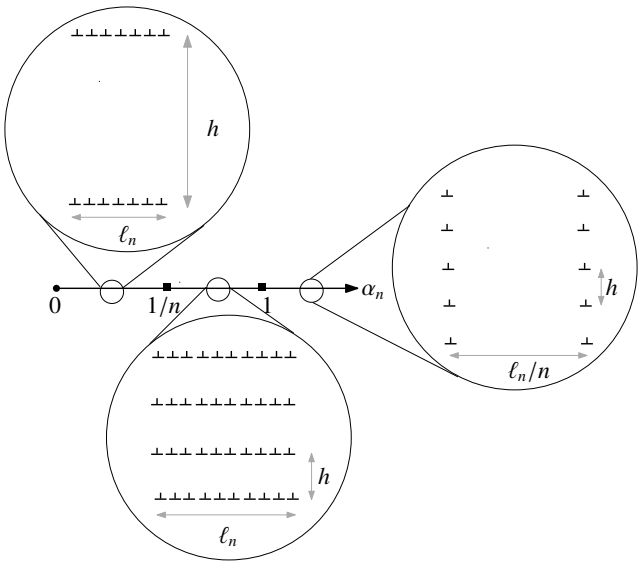

Figure 5: Possible scalings for the parameter α_n and some of the corresponding configurations.

the five regimes defined above we derive the following expressions for the dislocation energy in terms of this limiting, continuous density ρ:

(1) Subcritical regime: $$E^{(1)}(\rho) = -\frac{1}{2\pi^2}\int_0^\infty\int_0^\infty \log|x-y|\,\rho(x)\rho(y)dxdy + \int_0^\infty x\rho(x)dx;$$

(2) First critical regime: $$E^{(2)}(\rho) = \frac{1}{2}\int_0^\infty\int_0^\infty V(x-y)\rho(x)\rho(y)dxdy + \int_0^\infty x\rho(x)dx;$$

(3) Intermediate regime: $$E^{(3)}(\rho) = \frac{1}{6\pi}\int_0^\infty \rho^2(x)dx + \int_0^\infty x\rho(x)dx;$$

(4) Second critical regime: $$E^{(4)}(\rho) = \int_0^\infty \sum_{k=1}^{\infty} V\left(\frac{k}{\rho(x)}\right)\rho(x)dx + \int_0^\infty x\rho(x)dx;$$

(5) Supercritical regime: $$E^{(5)}(\rho) = \int_0^\infty x\rho(x)dx \quad \text{if } \rho \le 1.$$

The internal stresses associated to the continuum dislocation energies above will be derived in Section 4. Their dimensional counterparts will be introduced in Section 5, where they will be compared with alternative expressions for the internal stress proposed in the engineering literature.

We notice that the dislocation density ρ plays the same role as the curl of the plastic strain in strain gradient theories. It is therefore interesting to compare the interaction energies we derived with *defect energies* in strain gradient crystal plasticity models (see Section 5).

4. Derivation of the upscaled internal stress

In this section we derive, for each of the cases (1)-(5) above, the expressions of the pile-up length ℓ_n in terms of the parameters of the problem; moreover, we motivate heuristically why these are the right ones, and how the resulting limit expressions for the energy and the internal stress arise. In the companion paper [13] we prove that, for the expressions of ℓ_n derived here, the rescaled energy E_n converges as $n \to \infty$.

A convenient method to determine the scaling of ℓ_n is by requiring that both terms of the energy (8) are of the same order. As it turns out, the correct scaling can be determined by only considering the special, uniformly spaced configuration $x_i := i/n$. This choice is suggested by the convexity of the interaction energy V and is proved rigorously in [13].

Note that for this trial configuration the second term in (8) is always of order one, and therefore we will require that the choice of ℓ_n makes the first term in (8) also of order one. By this analysis we will relate ℓ_n and α_n to the parameters h, σ, K and n. In particular, we will relate ℓ_n and α_n to a single dimensionless parameter β_n defined as

$$\beta_n := \sqrt{\frac{K}{n\sigma h}}. \tag{9}$$

From the definition of β_n it follows that K, σ, and h may depend on n. This is the case, for instance, if the number of dislocations n increases because the density of Frank-Read sources increases, since then one would expect that the average slip plane spacing h should simultaneously decrease with n. We will further motivate our choice of β_n as scaling parameter in Section 5.

We now consider each of the five regimes separately. In every case we validate the continuum upscaled model by comparing its predictions with the solution of the discrete model.

4.1. Subcritical regime $\alpha_n \ll \frac{1}{n}$: derivation of the upscaled internal stress

In this section we consider the extreme case $\alpha_n \ll \frac{1}{n}$, or equivalently, $\frac{\ell_n}{h} \ll 1$, i.e., the case where the length ℓ_n of the pile-up region is much smaller than the in-wall dislocation spacing. In this case the in-plane interaction is much stronger than the in-wall interaction, i.e., the equivalent continuum formulation will not *sense* the walls and the result will correspond to the case of a single slip plane rather than infinite walls of dislocations.

This can be seen heuristically by comparing our model with the single slip plane case considered by e.g. Eshelby, Frank and Nabarro (EFN) in [9]. In the EFN model the equilibrium positions of n dislocations (as opposed to walls) in a single slip plane (under an applied stress σ that pushes them towards the barrier) are described by equations similar to (3), where the interaction potential is $\psi(t) := 1/\pi^2 t$. In Figure 6 we plot the discrete density ρ^d corresponding to the minimisers $x \in \mathbb{R}^n$ of the energy (14), for $\beta_n \ll \frac{1}{n}$, and of the EFN energy, where $\rho^d(x_i) := 1/(x_i - x_{i-1})$. The discrete densities of the two models show perfect agreement.

4.1.1. Heuristics for the scaling of the discrete energy

As described above, we will identify ℓ_n and α_n and the corresponding rescaling of the energy in (8) by requiring that the two terms of the discrete energy E_n are of the same order and bounded when calculated for the uniformly-spaced configuration. Since the second term in (8) is of order one, we need to impose that also the first term of the energy is of order one, i.e.,

$$\frac{K}{n\sigma h \alpha_n} \sum_{k=1}^{n} V(\alpha_n k) \sim 1. \tag{10}$$

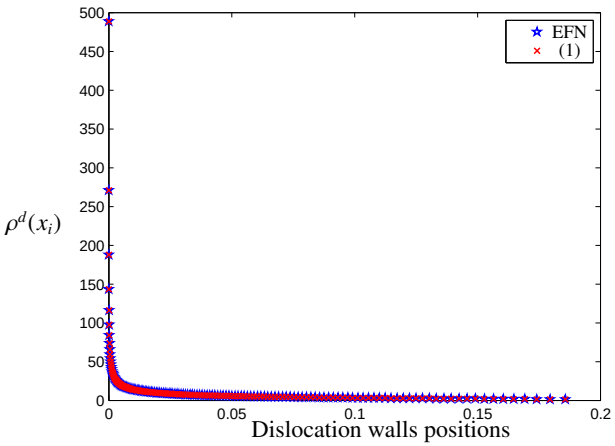

Figure 6: Comparison between the optimal discrete density in the EFN model and in (14), in the subcritical scaling regime (1). Here $n = 150$ and $\beta_n = \frac{4}{n\sqrt{n}} \left(\ll \frac{1}{n} \right)$. The stars and crosses completely coincide.

Since for this rescaling $n\alpha_n \ll 1$, the argument of V in (10) is small, as $\alpha_n k \leq \alpha_n n \ll 1$. Therefore we substitute for V in (10) its asymptotic expansion close to zero,

$$V(s) \sim \frac{1 - \log 2\pi s}{\pi^2}, \quad \text{for } s > 0.$$

Using this approximation in (10) we find that we should require that

$$\frac{K}{n\sigma h \alpha_n} \sum_{k=1}^{n} \left[\frac{1 - \log(2\pi\alpha_n k)}{\pi^2} \right] \sim 1. \tag{11}$$

As it stands, this condition would give rise to a wrong choice of ℓ_n and α_n. This is because the expression between brackets is dominated by a constant term, and this constant term is irrelevant for the equilibrium equations (since it vanishes upon differentiation). We therefore introduce the renormalized energy density $\hat{V}_n(t) := V(t) + \frac{-1+\log(2\pi n\alpha_n)}{\pi^2}$ in which we have subtracted this large constant. In terms of $\hat{V}_n$ the bound (11) on the energy becomes

$$-\frac{1}{\pi^2} \frac{K}{n\sigma h \alpha_n} \sum_{k=1}^{n} \log\left(\frac{k}{n}\right) \sim 1.$$

Simple computations show that

$$\frac{K}{n\sigma h \alpha_n} \sum_{k=1}^{n} \log\left(\frac{k}{n}\right) = \frac{K}{\sigma h \alpha_n} \left[\frac{1}{n} \sum_{k=1}^{n} \log\left(\frac{k}{n}\right) \right] \sim \frac{K}{\sigma h \alpha_n}, \tag{12}$$

since the term in square brackets is the Riemann sum for the integral $\int_0^1 \log(t)\, dt = 1$. Hence the bound on the energy reduces to the requirement that $\frac{K}{\sigma h \alpha_n} \sim 1$. This bound provides the following expressions for the aspect ratio α_n and for the length ℓ_n of the pile-up region in terms of the parameters σ, h, K and n (or in terms of the dimensionless parameter β_n defined in (9)):

$$\alpha_n^{(1)} \sim \frac{K}{\sigma h} = n\beta_n^2; \quad \ell_n^{(1)} \sim \frac{Kn}{\sigma} = n^2 \beta_n^2 h. \tag{13}$$

The scaling regime $\alpha_n \ll \frac{1}{n}$ can be equivalently formulated in terms of β_n and corresponds to $\beta_n \ll \frac{1}{n}$. From (8), using (13), we obtain the scaling of the discrete energy in the subcritical regime, which reads

$$E_n^{(1)}(x) := \frac{1}{n^2} \sum_{k=1}^{n} \sum_{j=0}^{n-k} \hat{V}_n \left(n^2 \beta_n^2 (x_{j+k} - x_j) \right) + \frac{1}{n} \sum_{j=0}^{n} x_j. \tag{14}$$

Note that $\hat{V}_n$ can be expressed in terms of β_n as $\hat{V}_n(t) = V(t) + \frac{-1+\log(2\pi n^2 \beta_n^2)}{\pi^2}$.

4.1.2. Continuum limit: derivation of the internal stress

We can rewrite the sums in (14) as integrals in terms of the discrete dislocation density $\rho_n := \frac{1}{n} \sum_{i=1}^{n} \delta_{x_i}$, namely

$$E_n^{(1)}(x) = \frac{1}{2} \int_0^\infty \int_0^\infty \hat{V}_n \left(n^2 \beta_n^2 (x - y) \right) \rho_n(x) \rho_n(y) dx dy + \int_0^\infty x \rho_n(x) dx. \tag{15}$$

In the previous formula we wrote the integral on $(0, \infty)$ since the wall positions x_i are in $(0, \infty)$. By the definition of $\hat{V}_n$ and since $n\beta_n \ll 1$ in this regime, we have that $\hat{V}_n \left(n^2 \beta_n^2 s \right) \sim -\frac{1}{\pi^2} \log |s|$. Substituting this expression in (15) we have

$$E_n^{(1)}(x) \simeq -\frac{1}{2\pi^2} \int_0^\infty \int_0^\infty \log |x - y| \, \rho_n(x) \rho_n(y) dx dy + \int_0^\infty x \rho_n(x) dx. \tag{16}$$

For a large number of walls, i.e., as $n \to \infty$, ρ_n converges to a continuum density ρ and the discrete energy $E_n^{(1)}$ converges to the continuum functional $E^{(1)}$ defined as:

$$E^{(1)}(\rho) := -\frac{1}{2\pi^2} \int_0^\infty \int_0^\infty \log |x - y| \, \rho(x) \rho(y) dx dy + \int_0^\infty x \rho(x) dx, \tag{17}$$

(see [13] for more details). The analogy with the discrete model is completed by the Euler-Lagrange equation associated with (17), which is an integral equation of the following form:

$$-\frac{1}{\pi^2} \int_0^\infty \frac{\rho(y)}{|x - y|} dy + 1 = 0, \tag{18}$$

for every $x \in (0, \infty)$. This equation is to be interpreted as a Cauchy principal-value integral (see e.g. [25, Ch. 2]). Alternatively, we can rewrite the equation (18) in the compact form

$$\frac{1}{\pi^2} \log * \partial_x \rho + 1 = 0. \tag{19}$$

Since the continuum equation (19) is the limit of a discrete system of the form $\sigma_i^{\text{int}} - \sigma = 0$, it can be interpreted as the dimensionless form of $\sigma_{\text{int}}^{(1)} - \sigma = 0$. Hence, the expression for the dimensionless internal stress we obtained is

$$\sigma_{\text{int}}^{(1)} = -\frac{1}{\pi^2} \log * \partial_x \rho. \tag{20}$$

4.1.3. Comparison Discrete vs Continuum

In Figure 7 we numerically compare the discrete density obtained by minimising the discrete energy (14) for $\beta_n \ll \frac{1}{n}$ and for large n with the solution of the continuum equation (19).

We note that the continuum equation (19) can be solved by means of the Hilbert transform, and it has a closed-form solution, found in [21] (see also [30]).

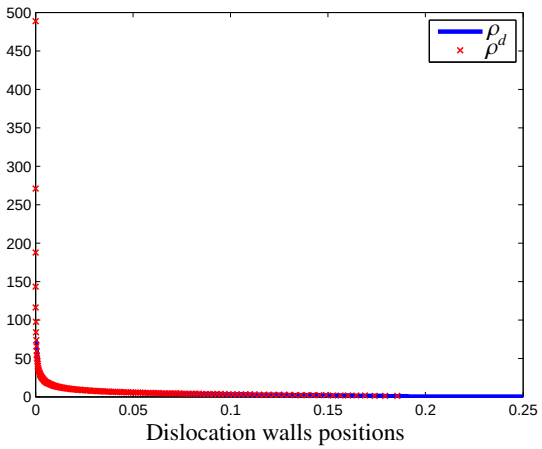

Figure 7: Comparison of the discrete and continuous pile-ups, for $n = 150$ and $\beta_n = 6/(n\sqrt{n})$. The continuum dimensionless density ρ minimizes $E^{(1)}$; the discrete dimensionless density ρ^d is calculated by minimizing $E_n^{(1)}$ over all x_i, and defining $\rho^d(x_i) := 1/(x_i - x_{i-1})$. Both are normalized such that the total density equals 1.

4.2. First critical regime $\alpha_n \sim \frac{1}{n}$: derivation of the upscaled internal stress

This regime corresponds to $\ell_n \sim h$, i.e., to the case where the length of the pile-up region is of the same order as the vertical dislocation spacing h and consequently, for large n, the horizontal wall-wall spacing is much smaller than h. Unlike the previous case, we cannot expect that the vertical interactions can be neglected and that the stress exerted by a wall is equivalent to the stress generated by a single dislocation. Qualitatively, though, the optimal dislocation density exhibits a sharp increase close to the obstacle, as in the previous case, and a fast decay at infinity.

4.2.1. Heuristics for the scaling of the discrete energy

Similarly as in the previous scaling regime, imposing that both terms of the discrete energy E_n in (8) are bounded and of the same order reduces to the condition

$$1 \sim \frac{K}{n^2\sigma h\alpha_n}\sum_{k=1}^{n}\sum_{j=0}^{n-k} V(\alpha_n k) \sim \frac{K}{n\sigma h\alpha_n^2}\left[\alpha_n \sum_{k=1}^{n} V(\alpha_n k)\right]. \tag{21}$$

Since for this scaling $n\alpha_n \sim 1$ as $n \to \infty$, the term in square brackets is of the same order as the Riemann sum for the integral $\int_0^1 V(t)dt < \infty$. Therefore (21) becomes

$$\frac{K}{n\sigma h\alpha_n^2} \sim 1, \tag{22}$$

which leads to the following expressions for α_n and ℓ_n (by using also (9)):

$$\alpha_n^{(2)} \sim \sqrt{\frac{K}{n\sigma h}} = \beta_n, \qquad \ell_n^{(2)} \sim \sqrt{\frac{Knh}{\sigma}} = n\beta_n h. \tag{23}$$

Note that by (23) we can directly reformulate the scaling regime as $\beta_n \sim \frac{1}{n}$. More precisely, this corresponds to $\beta_n = \frac{c_n}{n}$, for some $c_n \sim 1$ ($c_n \to c$ as $n \to \infty$). The rescaling of the energy (8)

obtained in this case is therefore

$$E_n^{(2)}(x) := \frac{c_n}{n^2} \sum_{k=1}^{n} \sum_{j=0}^{n-k} V\left(c_n(x_{j+k} - x_j)\right) + \frac{1}{n} \sum_{j=0}^{n} x_j. \tag{24}$$

4.2.2. Continuum limit: derivation of the internal stress

Rewriting the energy (24) in terms of the empirical measure $\rho_n = \frac{1}{n} \sum_{i=1}^{n} \delta_{x_i}$ we obtain

$$E_n^{(2)}(x) = \frac{c_n}{2} \int_0^\infty \int_0^\infty V(c_n(x-y))\rho_n(x)\rho_n(y)dxdy + \int_0^\infty x\rho_n(x)dx. \tag{25}$$

For a large number of walls, i.e., as $n \to \infty$, ρ_n converges to a continuum density ρ, $c_n \to c$, and the energy $E_n^{(2)}(x)$ converges to the continuum functional $E^{(2)}$ defined as:

$$E^{(2)}(\rho) := \frac{c}{2} \int_0^\infty \int_0^\infty V(c(x-y))\rho(x)\rho(y)dxdy + \int_0^\infty x\rho(x)dx. \tag{26}$$

The equilibrium dislocation density ρ is the solution of the Euler-Lagrange equation associated with the functional $E^{(2)}$, i.e., the solution of the integral equation

$$c \int_0^\infty V(c(x-y))\partial_y\rho(y)dy + 1 = 0 \tag{27}$$

for every $x \in (0, \infty)$, or, equivalently,

$$V_c * \partial_x\rho + 1 = 0, \tag{28}$$

where $V_c(s) := cV(cs)$. This equation is the mesoscopic equilibrium equation $\sigma_{\text{int}}^{(2)} - \sigma = 0$ in its non-dimensional form. Hence, the dimensionless internal stress obtained from this rescaling is

$$\sigma_{\text{int}}^{(2)} = -V_c * \partial_x\rho.$$

We note that, as for the previous scaling regime, also in this case the continuum equilibrium equation is a singular integral equation. The main difference is that whereas in the rescaling case (1) we could approximate V with its limit behaviour near zero (namely its logarithmic behaviour), here the complete energy density V enters the limit functional (26) and the equilibrium equation (28); the scaling constant $c = \lim_{n\to\infty} n\beta_n$ enters the expression as well.

4.2.3. Comparison Discrete vs Continuum

In Figure 8 we show the agreement between the solution of the upscaled continuum equation (27) and the minimiser of the discrete energy (24), for a large number n of dislocation walls.

4.3. Intermediate regime $\frac{1}{n} \ll \alpha_n \ll 1$: derivation of the upscaled internal stress

This scaling regime corresponds to the *intermediate* situation in which the pile-up length ℓ_n is much larger than the vertical spacing h while the average in-plane distance between consecutive dislocations is, on the contrary, much smaller than h.

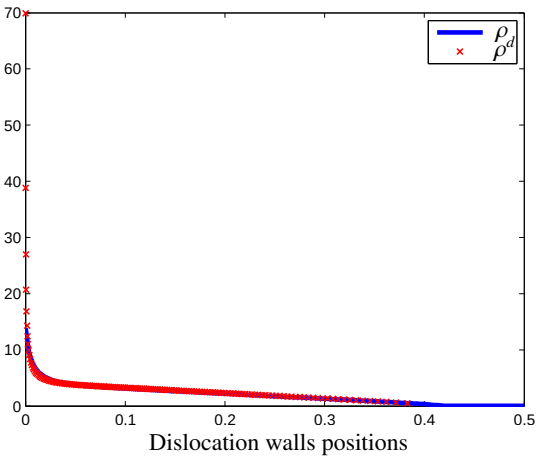

Figure 8: Comparison of the discrete and continuous pile-ups for $E_n^{(2)}$ and $E^{(2)}$, for $n = 150\,\beta_n = 5/n$.

4.3.1. Heuristics for the scaling of the discrete energy

Using again the equispaced wall distribution $x_i = \frac{i}{n}$ as a test for the discrete energy E_n in (8) and proceeding as in the previous cases leads to the following requirement

$$1 \sim \frac{K}{n^2\sigma h\alpha_n}\sum_{k=1}^{n}\sum_{j=0}^{n-k} V(\alpha_n k) \sim \frac{K}{n\sigma h\alpha_n^2}\left[\alpha_n \sum_{k=1}^{n} V(\alpha_n k)\right]; \tag{29}$$

since, by assumption, $\alpha_n \to 0$ and $n\alpha_n \to \infty$, the term in the square brackets is a Riemann sum for the integral $\int_0^\infty V(t)dt = 1/6\pi$. Hence the condition (29) on the energy is equivalent to

$$\frac{K}{n\sigma h\alpha_n^2} \sim 1, \tag{30}$$

which is identical to (22) and therefore leads to the same expressions for $\alpha_n^{(3)}$ and $\ell_n^{(3)}$ as for $\alpha_n^{(2)}$ and $\ell_n^{(2)}$ in (23). In particular, also in this case $\alpha_n^{(3)} \sim \beta_n$; in terms of β_n the scaling regime is $\frac{1}{n} \ll \beta_n \ll 1$. Using (30), the rescaling of the energy (8) becomes, for $\frac{1}{n} \ll \beta_n \ll 1$,

$$E_n^{(3)}(x) := \frac{\beta_n}{n}\sum_{k=1}^{n}\sum_{j=0}^{n-k} V\left(n\beta_n(x_{j+k} - x_j)\right) + \frac{1}{n}\sum_{j=0}^{n} x_j. \tag{31}$$

4.3.2. Continuum limit: derivation of the internal stress

In terms of the distribution $\rho_n = \frac{1}{n}\sum_{i=1}^{n}\delta_{x_i}$, the energy (31) can be rewritten as

$$E_n^{(3)}(x) = \frac{1}{2}\,n\beta_n \int_0^\infty\int_0^\infty V\left(n\beta_n(x-y)\right)\rho_n(x)\rho_n(y)dxdy + \int_0^\infty x\rho_n(x)dx. \tag{32}$$

We note that, since $n\beta_n \to \infty$, $n\beta_n V(n\beta_n s) \to \left(\int_{-\infty}^{\infty} V\right)\delta_0 = (3\pi)^{-1}\delta_0$; hence for $n \to \infty$ the energy $E_n^{(3)}$ converges to the continuum energy $E^{(3)}$ defined as:

$$E^{(3)}(\rho) := \frac{1}{6\pi}\int_0^\infty \rho^2(x)dx + \int_0^\infty x\rho(x)dx. \tag{33}$$

The dislocation density ρ minimising $E^{(3)}$ is the solution of the Euler-Lagrange equation associated to the dimensionless functional $E^{(3)}$, i.e.,

$$\frac{1}{3\pi}\partial_x\rho + 1 = 0. \tag{34}$$

We notice that unlike the previous scaling regimes the continuum equilibrium equation in this case is local. Moreover, from (34) it is clear that the optimal dislocation density is linear. This was observed numerically in [14] and proved in [18] using formal methods.

Equation (34) is the mesoscopic equilibrium equation $\sigma^{(3)}_{\text{int}} - \sigma = 0$ in its non-dimensional form. Hence, the dimensionless internal stress obtained from this rescaling is

$$\sigma^{(3)}_{\text{int}} = -\frac{1}{3\pi}\partial_x\rho.$$

4.3.3. Comparison Discrete vs Continuum

In Figure 9 we compare numerically the discrete density corresponding to a minimiser of the rescaled energy $E^{(3)}_n$ in (31) and the solution of the continuum equation (34). We notice that the agreement between the two densities is perfect in the *bulk*, sufficiently far from the boundary of the pile-up region, where the occurrence of boundary layers is expected.

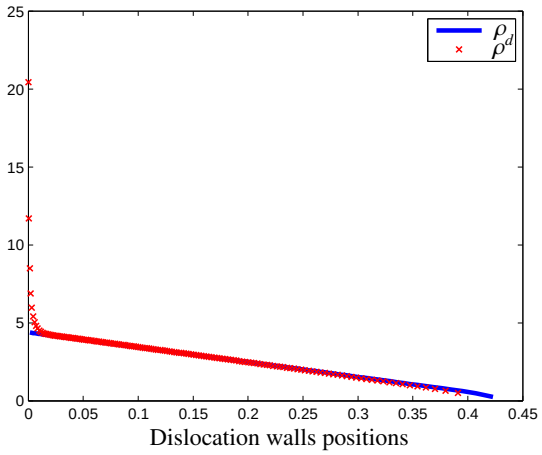

Figure 9: Comparison of the discrete and continuous pile-ups for $E^{(3)}_n$ and $E^{(3)}$, for $n = 150$ and $\beta_n = 1/\sqrt{n} = 1/\sqrt{150}$.

4.4. Second critical regime $\alpha_n \sim 1$: derivation of the upscaled internal stress

The scaling regime $\alpha_n \sim 1$ corresponds to configurations where the in-plane and the in-wall distances between consecutive dislocations are of the same order. This is a special situation as compared to cases (1)–(3), where the aspect ratio is small (hence the in-plane interaction is stronger than the in-wall interaction) and the opposite case (5). For this reason we look at case (4) as the main critical case and we expect to get a better insight in the problem from its analysis.

4.4.1. Heuristics for the scaling of the discrete energy

Proceeding as in the previous cases leads to the requirement (29), where this time $\alpha_n \sim 1$:

$$1 \sim \frac{K}{n^2\sigma h\alpha_n}\sum_{k=1}^{n}\sum_{j=0}^{n-k} V(\alpha_n k) \sim \frac{K}{n\sigma h\alpha_n}\sum_{k=1}^{n} V(\alpha_n k).$$

Since $\sum_{k=1}^{\infty} V(k) < \infty$, the boundedness of the energy reduces to the following condition:

$$\frac{K}{n\sigma h\alpha_n} \sim 1. \tag{35}$$

From (35) we obtain the following expressions for the aspect ratio α_n and the pile-up length ℓ_n:

$$\alpha_n^{(4)} = \frac{K}{n\sigma h} = \beta_n^2, \quad \ell_n^{(4)} = \frac{K}{\sigma}. \tag{36}$$

The scaling regime corresponds to $\beta_n \sim 1$. Hence we can rescale the energy (8) as in (31), i.e.,

$$E_n^{(4)}(x) := \frac{\beta_n}{n}\sum_{k=1}^{n}\sum_{j=0}^{n-k} V\Big(n\beta_n(x_{j+k} - x_j)\Big) + \frac{1}{n}\sum_{j=0}^{n} x_j, \tag{37}$$

where now $\beta_n \sim 1$ (note that (36) suggests β_n^2 instead of β_n, but in this regime $\beta_n \sim \beta_n^2$).

4.4.2. Continuum limit: derivation of the internal stress

The derivation of the continuum energy in this regime is quite different from the one outlined in Sections 4.1-4.3. While for $\alpha_n \ll 1$ the sum over k in the discrete energy (8) gives rise to an integral term, for $\alpha_n \sim 1$ this is no longer the case. Here we sketch the upscaling method (setting $\beta_n = 1$ for simplicity) and refer to [13] for the complete proof.

The idea in this case is to view the positions of the walls x_i as the deformed positions from an initial equispaced wall configuration of $n+1$ walls in $(0,1)$ via a deformation map ξ_n, i.e., $x_i = \xi_n\left(\frac{i}{n}\right)$. The map ξ_n can be extended in the whole range $(0,1)$ as the affine interpolation of $x_1, \dots, x_n$ (see Figure 10). In this way we can formally read the argument of V in (37) as a difference quotient of ξ_n, i.e.,

$$V\Big(n(x_{j+k} - x_j)\Big) = V\left(k\,\frac{x_{j+k} - x_j}{k/n}\right) \sim V\left(k\,\xi_n'\left(\frac{j}{n}\right)\right).$$

Hence for the discrete energy (37) we have

$$E_n^{(4)}(x) = \sum_{k=1}^{n}\left\{\frac{1}{n}\sum_{j=0}^{n-k} V\left(k\,\xi_n'\left(\frac{j}{n}\right)\right)\right\} + \frac{1}{n}\sum_{j=0}^{n}\xi_n\left(\frac{j}{n}\right), \tag{38}$$

which for $n \to \infty$ converges to the continuum functional

$$E^{(4)}(\xi) := \sum_{k=1}^{\infty}\int_0^1 V(k\xi'(s))\,ds + \int_0^1 \xi(s)\,ds, \tag{39}$$

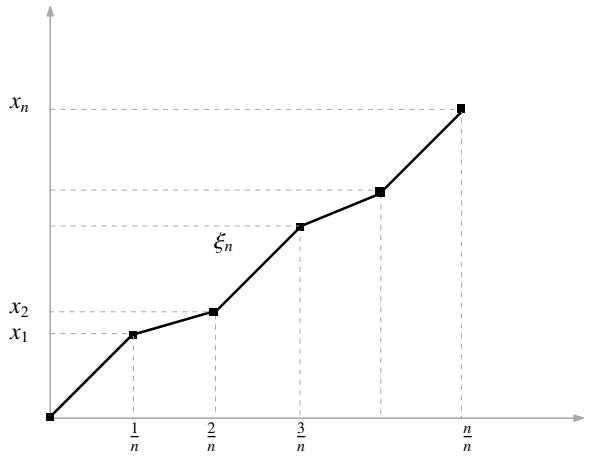

Figure 10: Interpolation of the positions of the walls.

where ξ is the limit of the interpolations and the integrals are the limits of the Riemann sums in (38). Since we are interested in a continuum model in terms of the dislocation density rather than the limit positions it remains to change variables in the energy (39), using the relation

$$\rho(\xi(s)) := \frac{1}{\xi'(s)}, \tag{40}$$

which is the continuum version of the discrete relation (4). The relation (40) entails $ds = \rho(x)\,dx$. Changing variables in (39) leads to an energy depending on the dislocation density, namely

$$E^{(4)}(\rho) = \int_0^\infty V_{\text{eff}}\left(\frac{1}{\rho(x)}\right)\rho(x)dx + \int_0^\infty x\rho(x)dx, \tag{41}$$

where $V_{\text{eff}}(t) := \sum_{k=1}^{\infty} V(kt)$, for every $t \in \mathbb{R}$. The dislocation density ρ minimising the energy (41) is the solution of the Euler-Lagrange equation associated to the functional $E^{(4)}$, i.e.,

$$-\frac{\partial_x \rho}{\rho^3}\,\varphi'_{\text{eff}}\left(\frac{1}{\rho}\right) + 1 = 0, \tag{42}$$

where $\varphi_{\text{eff}}(t) := \sum_{k=1}^{\infty} k\varphi(kt)$, for every $t \in \mathbb{R}$. Note that the infinite sum in φ_{eff} results form having taken into account all dislocation interactions in the discrete model: the term $k = 1$ corresponds to interactions among nearest neighbours, the term $k = 2$ to next-to-nearest neighbour interactions and so on. Moreover, whereas in the previous cases the dislocation walls were sufficiently close to regard them as a continuum density, here the discrete interactions prevail.

Equation (42) is again the mesoscopic equilibrium equation $\sigma^{(4)}_{\text{int}} - \sigma = 0$ in its non-dimensional form. Hence, the dimensionless internal stress obtained for this rescaling is

$$\sigma^{(4)}_{\text{int}} = \frac{\partial_x \rho}{\rho^3}\,\varphi'_{\text{eff}}\left(\frac{1}{\rho}\right).$$

Remark 4.1. We show here how (42) can be heuristically derived starting from the original, dimensional equilibrium equations (3). We will focus on a general k-th term in φ_{eff}.

For a dislocation located at a point $\tilde{x}$, we denote by d_k the average distance to its k-th neighbours, i.e., $d_k \sim \frac{k}{\tilde{\rho}}$. The actual distance $d_k^{\pm}(\tilde{x})$ between the dislocation at $\tilde{x}$ and its k-th neighbour on the right and on the left are given by the following corrections of d_k, namely

$$d_k^+ \sim \frac{k}{\tilde{\rho}} + \left(-\frac{1}{\tilde{\rho}^2}\frac{\partial\tilde{\rho}}{\partial\tilde{x}}\right)\left(\frac{1}{2}\,\frac{k}{\tilde{\rho}}\right), \qquad d_k^- \sim \frac{k}{\tilde{\rho}} + \left(-\frac{1}{\tilde{\rho}^2}\frac{\partial\tilde{\rho}}{\partial\tilde{x}}\right)\left(-\frac{1}{2}\,\frac{k}{\tilde{\rho}}\right).$$

Therefore, the distance between its k-th neighbours is

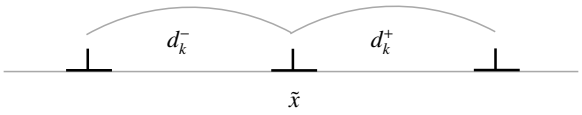

Figure 11: k-interactions.

$$\Delta d \sim -\frac{k}{\tilde{\rho}^3}\partial_{\tilde{x}}\tilde{\rho}.$$

According to the previous relations, the force exerted on the dislocation at $\tilde{x}$ by the k-th neighbour dislocation on the right and on the left are, respectively,

$$\frac{K}{h}\varphi\left(\frac{d_k^+}{h}\right) \sim \frac{K}{h}\left[\varphi\left(\frac{d_k}{h}\right) + \frac{1}{2h}\,\varphi'\left(\frac{d_k}{h}\right)\Delta d\right],$$
$$\frac{K}{h}\varphi\left(\frac{d_k^-}{h}\right) \sim \frac{K}{h}\left[\varphi\left(\frac{d_k}{h}\right) - \frac{1}{2h}\,\varphi'\left(\frac{d_k}{h}\right)\Delta d\right].$$

The net force exerted on the dislocation at $\tilde{x}$ by its k-th neighbours is, therefore,

$$\frac{K}{h}\Delta\varphi \sim \frac{K}{h^2}\varphi'(d_k)\Delta d = -\frac{K}{h^2}\frac{k}{\tilde{\rho}^3}\,\partial_{\tilde{x}}\tilde{\rho}\;\varphi'\left(\frac{k}{\tilde{\rho}}\right),$$

which is exactly the k-th term in the dimensional stress (53).

4.4.3. Comparison Discrete vs Continuum

In Figure 12 we show the agreement between the solution of the continuum equation (42) and the minimiser of the rescaled discrete energy (37), for $\beta_n \sim 1$. Also in this case we can notice the occurrence of boundary layers at the left end of the pile-up region.

4.5. Supercritical regime $\alpha_n \gg 1$: derivation of the upscaled internal stress

In this scaling regime the in-plane dislocation distance is much larger than the in-wall distance, and therefore the in-plane interaction is quite weak. In this case we can prove that truncating the in-plane interactions to the first neighbours (but keeping the walls) leads to the right limit model, unlike the previous cases, where all interactions had to be accounted for.

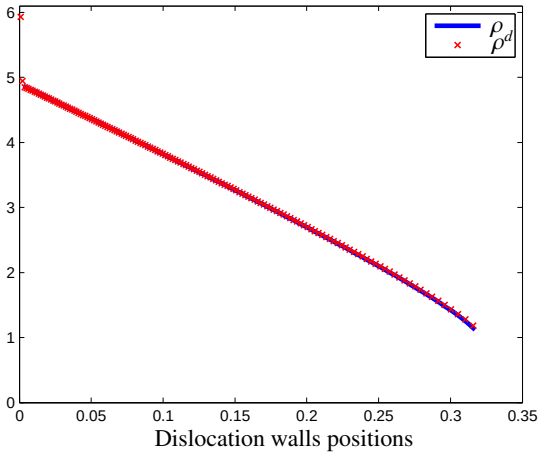

Figure 12: Comparison of the discrete and continuous pile-ups for $E_n^{(4)}$ and $E^{(4)}$, with $n = 150$ and $\beta_n = 1$.

4.5.1. Heuristics for the scaling of the discrete energy

We first note that the energy (8) is always larger than its truncation to first neighbours, i.e.,

$$E_n(x) \geq \frac{K}{n^2\sigma h\alpha_n} \sum_{j=0}^{n-1} V\left(n\alpha_n(x_{j+1} - x_j)\right) + \frac{1}{n}\sum_{j=0}^{n} x_j, \tag{43}$$

regardless of the scaling regime. In the case $\alpha_n \gg 1$ the bound (43) is optimal, meaning that the energy E_n and its first order truncation give rise to the same continuum model (see [13]). This is in contrast with what happens in *all* the previous cases (1)–(4), where the truncation of the interactions would produce a completely different (and wrong) result (see also the discussion in [28]). To obtain the energy scaling we use once more the equispaced wall configuration $x_i = \frac{i}{n}$ as a test configuration. Then the bound on the energy truncated to the first neighbours reduces to

$$\frac{K}{n\sigma h\alpha_n} V(\alpha_n) \sim 1. \tag{44}$$

Since $\alpha_n \gg 1$, we can substitute for V its asymptotic behaviour at infinity; by (6) we have

$$V(s) \sim \frac{2}{\pi} s e^{-2\pi s} \quad \text{as} \quad s \to \infty. \tag{45}$$

Therefore, using the previous relation, the bound (44) becomes

$$\frac{K}{n\sigma h}\frac{2}{\pi} e^{-2\pi\alpha_n} \sim 1.$$

In terms of α_n, and using (13), the previous relation entails

$$\alpha_n^{(5)} \sim \frac{1}{2\pi}\log\left(\frac{2}{\pi}\frac{K}{nh\sigma}\right) = \frac{1}{2\pi}\log\left(\frac{2\beta_n^2}{\pi}\right), \qquad \ell_n^{(5)} = nh\alpha_n \sim \frac{nh}{2\pi}\log\left(\frac{2\beta_n^2}{\pi}\right). \tag{46}$$

Therefore, the energy scaling for $\alpha_n \gg 1$ can be rephrased in terms of β_n as $\beta_n \gg 1$, and the corresponding energy scaling in the regime $\beta_n \gg 1$ is

$$E_n^{(5)}(x) := \frac{2\pi\beta_n^2}{n\log\left(\frac{2\beta_n^2}{\pi}\right)} \sum_{k=1}^{n}\sum_{j=0}^{n-k} V\left(\frac{n}{2\pi}\,\log\left(\frac{2\beta_n^2}{\pi}\right)(x_{j+k}-x_j)\right) + \frac{1}{n}\sum_{j=0}^{n} x_j. \tag{47}$$

For what follows it is convenient to introduce a new parameter $\gamma_n := \frac{1}{2\pi}\log\left(\frac{2\beta_n^2}{\pi}\right)$ (note that this scaling regime corresponds to $\gamma_n \gg 1$) and to rewrite (47) in terms of γ_n, namely

$$E_n^{(5)}(x) = \frac{\pi}{2}\frac{e^{2\pi\gamma_n}}{n\gamma_n}\sum_{k=1}^{n}\sum_{j=0}^{n-k} V\left(n\gamma_n(x_{j+k}-x_j)\right) + \frac{1}{n}\sum_{j=0}^{n} x_j. \tag{48}$$

4.5.2. Continuum limit: derivation of the internal stress

As in Section 4.4 we introduce the interpolation ξ_n of the positions of the walls. Since we expect the term $k = 1$ in the sum in (48) to be dominant we disregard the other terms in our formal derivation of the limit energy (for the rigorous proof we refer to [13]). We have, formally,

$$\begin{aligned} E_n^{(5)}(x) &\simeq \frac{\pi}{2}\frac{e^{2\pi\gamma_n}}{n\gamma_n}\sum_{j=0}^{n-1} V\left(\gamma_n\xi'\left(\frac{j}{n}\right)\right) + \frac{1}{n}\sum_{j=0}^{n}\xi\left(\frac{j}{n}\right) \\ &\simeq \frac{\pi}{2}\frac{e^{2\pi\gamma_n}}{\gamma_n}\int_0^1 V(\gamma_n\xi'(s))ds + \int_0^1 \xi(s)ds. \end{aligned}$$

By (45) we have that, for $s \in (0,1)$,

$$\frac{\pi}{2}\frac{e^{2\pi\gamma_n}}{\gamma_n}\,V(\gamma_n\xi'(s)) \sim \xi'(s)\,e^{2\pi(\gamma_n-\xi'(s))},$$

which is finite (actually zero) only if $\xi'(s) \geq 1$. In terms of the density ρ, using (40) the limit energy is the dimensionless continuum functional $E^{(5)}$ defined as:

$$E^{(5)}(\rho) = \int_0^\infty x\rho(x)dx \quad \text{if } \rho \leq 1, \tag{49}$$

and $+\infty$ otherwise. This limit functional is degenerate: it only is finite if the dislocations are sufficiently far apart. The optimal density in this case is the constant density 1 from $x = 0$ to $x = 1$, and density zero for $x \geq 1$ (see Figure 13).

4.5.3. Comparison Discrete vs Continuum

In this section we show the agreement between the minimiser of the discrete energy (47), for $\beta_n \gg 1$ and for large n, and the minimiser of the continuum energy (49). In Figure 13 we have plotted the piecewise constant optimal continuum density and the optimal discrete density for $n = 150$ and $\beta_n = 10^8$: we see that the discrete density approaches the value 1.

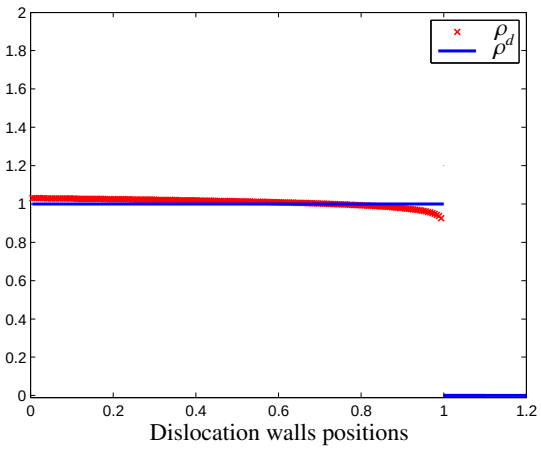

Figure 13: Optimal densities for $E_n^{(5)}$ and $E^{(5)}$, with $n = 150$ and $\beta_n = 10^8$.

5. Discussions and conclusion

This paper unravels the mechanical response of a system of walls of parallel edge dislocations on equidistant parallel slip planes. By implementing a rigorous mathematical limit procedure, we have identified five different parameter regimes, as the number n of walls tends to infinity. These regimes are characterized by the asymptotic behaviour of a single dimensionless parameter.

For each of these regimes we have identified the limiting internal stress that is generated by the dislocation density, and the structure of a pile-up of walls against a hard obstacle (see also Section 5.3). For two of the regimes the expressions that we obtain were known in the literature, and our results provide new insight by delineating the conditions under which these expressions are valid. The three other cases are new, and the corresponding behaviour has not been studied before.

Although the analysed wall configuration is highly simplified, the rigorous nature of this work implies that these results can be considered as a benchmark: any (possibly more general) model that describes the behaviour of large numbers of dislocations should reproduce at least the behaviour given by the results of this paper when applied to the corresponding idealised situation.

5.1. Transition between the different limit models.

The transition between the regimes (1)–(5) is *continuous* in terms of the energy. For example, the integrand in the first term of the continuum energy $E^{(2)}$ in (26) contains the term $c\,V(cs)$, which for c large (corresponding to a transition from regime (2) to regime (3)) converges to $\left(\int V\right)\delta$, which is indeed the term appearing in the energy $E^{(3)}$ in (33). If instead c is small (corresponding to the transition from regime (2) to regime (1)), then the logarithmic singularity of V appears, leading to the energy (17). The other transitions can be explained analogously.

5.2. Comparison with previous models

In this section we show how the expressions for the internal stress obtained in this paper, starting from an idealised discrete model, relate to some well-known models in the engineering literature. Our results offer a unifying approach for understanding these existing models: they

can all be derived by upscaling the same discrete model, but under different assumptions on the local arrangements of the dislocations, i.e., for different values of the aspect ratio β_n.

First of all we list the dimensional internal stresses obtained in the scaling regimes (1)–(4) (we omit (5) since the equilibrium equation is too degenerate to provide a useful expression for the internal stress), i.e.,

$$\text{(1) Subcritical regime} \qquad \beta_n \ll \frac{1}{n} : \qquad \sigma^{(1)}_{\text{int}}(\tilde{x}) = \frac{K}{\pi^2} \int_0^\infty \log|\tilde{x}-\tilde{y}| \partial_{\tilde{y}} \tilde{\rho}(\tilde{y})\, d\tilde{y}; \tag{50}$$

$$\text{(2) First critical regime} \qquad \beta_n \sim \frac{1}{n} : \qquad \sigma^{(2)}_{\text{int}}(\tilde{x}) = -K \int_0^\infty V\Big(\frac{\tilde{x}-\tilde{y}}{h}\Big) \partial_{\tilde{y}} \tilde{\rho}(\tilde{y})\, d\tilde{y}; \tag{51}$$

$$\text{(3) Intermediate regime} \qquad \frac{1}{n} \ll \beta_n \ll 1 : \qquad \sigma^{(3)}_{\text{int}}(\tilde{x}) = -\frac{Kh}{3\pi} \partial_{\tilde{x}} \tilde{\rho}; \tag{52}$$

$$\text{(4) Second critical regime} \qquad \beta_n \sim 1 : \qquad \sigma^{(4)}_{\text{int}}(\tilde{x}) = \frac{K}{h^2} \frac{1}{\tilde{\rho}^3} \varphi'_{\text{eff}}\Big(\frac{1}{h\tilde{\rho}}\Big)\, \partial_{\tilde{x}} \tilde{\rho}. \tag{53}$$

The continuous density $\tilde{\rho}$ above is the infinite-n limit of the discrete density $\tilde{\rho}^d$ introduced in (4).

As observed in Section 4.1, the back-stress $\sigma^{(1)}_{\text{int}}$ coincides with the one derived by Eshelby, Frank, and Nabarro [9] and Head and Louat [21]. The starting point of both works is a system of discrete equilibrium equations for n dislocations in one slip plane, which is different from the *walls* of dislocations that we consider. This translates into a system of discrete equilibrium equations of the form (3), with the single-slip-plane interaction potential $\psi(t) = 1/(\pi^2 t)$ instead of the the potential φ. We note that the interaction potential ψ is similar to φ for small values of t, but differs for larger values. This is consistent with the fact that the internal stress $\sigma^{(1)}_{\text{int}}$ has been obtained in the scaling regime $\beta_n \ll 1/n$, where all the dislocation walls are confined in a region that is small compared to the slip planes spacing h. Hence the in-plane interactions between dislocations are much stronger than the in-wall interactions. An approximation by a single-slip-plane setup is therefore appropriate. A comparison between the two discrete models in terms of the equilibrium densities is shown in Figure 6.

The internal stress $\sigma^{(3)}_{\text{int}}$ coincides, at least qualitatively, with the one proposed in [10] and derived phenomenologically from interactions among dislocations. In the quoted paper, however, the expression of the internal stress contains a length scale R (not explicitly determined), representing the spatial reach of the dislocations interactions. By matching the stress $\sigma^{(3)}_{\text{int}}$ in its dimensional form (52) with the one derived in [10] (see also [3]) we can determine the length scale R, namely $R \sim h$. Therefore R depends on the in-wall spacing h only.

In the special case $\beta_n = cn^{-1/2}$ for some constant c, the simple ordinary differential equation (34) characterising the equilibrium dislocation density in this regime has also been obtained (following a different method) in the recent paper [18], starting from the discrete system (3).

The other internal stresses $\sigma^{(2)}_{\text{int}}$, $\sigma^{(4)}_{\text{int}}$ and $\sigma^{(5)}_{\text{int}}$ were not obtained so far.

The expression for the internal stress proposed by Groma, Csikor, and Zaiser [16] is a special case. It has been derived under the assumption that the distance to a nearest neighbouring dislocation is independent of the direction in which it is found. In our formulation this corresponds to the second critical case (4), namely $\beta_n \sim 1$. Therefore it is interesting to compare the internal stress of [16] to $\sigma^{(4)}_{\text{int}}$ above. As it turns out, the internal stress of [16], which up to constants reads $\sigma^{(GCZ)}_{\text{int}} = -\partial_{\tilde{x}}\tilde{\rho}/\tilde{\rho}$, can be *formally* obtained from $\sigma^{(4)}_{\text{int}}$ by making two approximations. The

first consists in truncating the number of interacting dislocations to the nearest neighbours. We note that truncating the interactions to the first neighbours is equivalent to replacing the effective potential φ_{eff} (which is a sum whose k-th term corresponds to the interactions between k-th neighbours) with φ. This first simplification reduces the internal stress $\sigma_{\text{int}}^{(4)}$ above to

$$\sigma_{\text{int}} = \frac{K}{h^2}\frac{1}{\tilde{\rho}^3}\varphi'\left(\frac{1}{h\tilde{\rho}}\right)\partial_{\tilde{x}}\tilde{\rho}. \tag{54}$$

The second approximation that leads to the internal stress proposed in [16] is to substitute the force $\varphi(t)$ with its first-order Taylor-Laurent expansion close to zero, which coincides with the single-slip plane force $\psi(t) = 1/(\pi^2 t)$ used in [9, 21]. By using ψ instead of φ in (54) we obtain exactly (up to a constant) $\sigma_{\text{int}}^{(GCZ)} = -\partial_{\tilde{x}}\tilde{\rho}/\tilde{\rho}$.

The comparison between the interactions stresses φ_{eff}, φ and ψ is illustrated in Figure 14. From the figure it is clear that φ is a good approximation of φ_{eff} only for large values of its

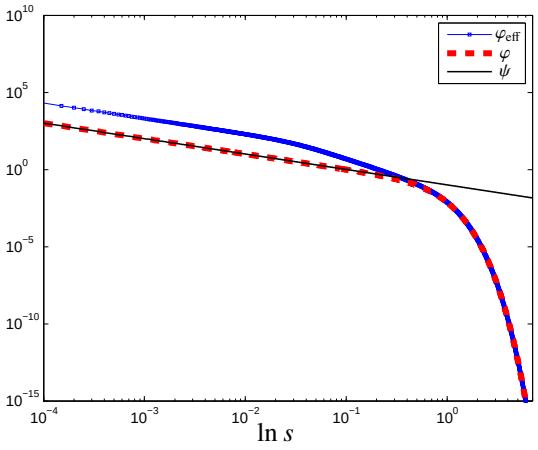

Figure 14: Interaction potentials φ_{eff}, φ and ψ in a log-log plot.

argument. Therefore the first approximation (54) is justified when $h\tilde{\rho}$ is small. This is exactly the case, though, when the second approximation is not allowed, since ψ and φ are close only near zero (corresponding to the opposite case of large $h\tilde{\rho}$). Therefore, although this derivation can formally be made, it can not be made rigorous, since the two approximations are mutually incompatible. More precisely, if first truncating to nearest neighbours (replacing φ_{eff} by φ) and then Taylor-expanding φ were a consistent combination, then the Taylor expansion of φ_{eff} and of

φ would be similar. However, this is not the case, since close to zero $\varphi(t) \approx \psi(t) = 1/\pi^2 t$, while [2]

$$\varphi_{\text{eff}}(t) \approx \frac{1}{2t^2} \int_{-\infty}^{\infty} V \qquad \text{as } t \to 0. \tag{55}$$

Close to zero, therefore, many neighbours are relevant, and nearest-neighbour truncation results in a large error.

The idea of deriving a continuum dislocation model from a discrete model of dislocation walls in a pile-up is also present in the work of Mesarovic and collaborators [2, 24]. Their approach consists in performing a two-step upscaling from the discrete dislocation model: first the dislocations are smeared out in the slip plane, but the discreteness is kept inside the wall; then the semi-discrete model obtained in the first step is upscaled in the vertical direction. We stress that there is no physical reason for performing the upscaling in the two directions separately. In fact, as the authors of the quoted papers correctly point out, the error between the predictions of the continuum model they obtain and the discrete model they start with (they refer to it as "coarsening error") is significant (this was already observed in [28]). Therefore, they need to correct *ad hoc* the resulting continuum model in order to match the predictions of the discrete model. The continuum model we obtain, instead, agrees perfectly with the discrete model we considered, and therefore we do not have to add any artificial terms to guarantee the matching.

It is also interesting to compare our upscaled interaction energies to *defect energies* proposed in strain gradient plasticity models (see e.g. [11] and [17]). We notice that our continuum dislocation density ρ plays the same role as the curl of the plastic strain in strain gradient plasticity models. Having this in mind, we can conclude that the interaction energy we obtain in the intermediate scaling regime is *exactly* the defect energy in [17], since it is quadratic in the dislocation density. The one-homogeneous defect energy in [11], instead, does not correspond to any of our limit models. We believe however that it represents a core energy rather than an interaction energy, while we only focus on interactions.

5.3. Pile-up behaviour: optimal density and pile-up length

The upscaled equilibrium density $\tilde{\rho}$ of a set of dislocation walls that is pushed against the obstacle at $\tilde{x} = 0$ solves the equation

$$\sigma_{\text{int}}^{(1-4)}(\tilde{x}) - \sigma = 0, \tag{56}$$

for the upscaled internal stresses listed in (50)-(53). We now analyse the behaviour of the dislocation density and comment on the length of the pile-up region in the different scalings.

[2] This follows from the two inequalities (since $s \mapsto s\varphi(s)$ is decreasing in $(0, \infty)$ and $\int_{-\infty}^{\infty} s\varphi(s) = \int_{-\infty}^{\infty} V$)

$$\varphi_{\text{eff}}(t) = \sum_{k=1}^{\infty} k\varphi(kt) \leq \sum_{k=1}^{\infty} \frac{1}{t^2} \int_{(k-1)t}^{kt} s\varphi(s)\, ds = \frac{1}{t^2} \int_0^{\infty} s\varphi(s)\, ds,$$

and

$$\varphi_{\text{eff}}(t) = \sum_{k=1}^{\infty} k\varphi(kt) \geq \sum_{k=1}^{\infty} \frac{1}{t^2} \int_{kt}^{(k+1)t} s\varphi(s)\, ds = \frac{1}{t^2} \int_t^{\infty} s\varphi(s)\, ds.$$

1. For the Subcritical regime, equation (56) has been solved by Head and Louat [21]:

$$\tilde{\rho}(\tilde{x}) = \frac{\sigma}{K}\sqrt{\frac{\ell - \tilde{x}}{\tilde{x}}}, \qquad \text{with } \ell = \frac{2nK}{\pi^2\sigma}.$$

   We notice that the length of the pile-up is independent of the wall spacing h. This is not surprising, since in this case only the in-plane interactions play a role, so the walls could be equivalently replaced by individual dislocations.
2. For the First critical regime, equation (56) has no explicit solution, to our knowledge.
3. In the Intermediate regime, the equilibrium density is given by

$$\tilde{\rho}(\tilde{x}) = \frac{2n}{\ell^2}(\ell - \tilde{x}), \qquad \text{with } \ell = \sqrt{\frac{2nKh}{3\pi\sigma}}.$$

4. In the Second critical regime we believe that equation (56) has no known explicit solution.
5. Finally, in the Supercritical regime, the equilibrium density $\tilde{\rho}$ is constant:

$$\tilde{\rho}(\tilde{x}) = \begin{cases} \ell^{-1} & \text{if } \tilde{x} \le \ell, \\ 0 & \text{otherwise,} \end{cases} \qquad \text{with } \ell = \frac{1}{2\pi}n^2 h\sigma \ln\Big(\frac{2K}{nh\sigma}\Big).$$

In the three explicit cases above, the parameter ℓ is exactly the pile-up length. Note that ℓ scales the same as the parameter ℓ_n (see (13), (23) and (46)), but the two differ by a numerical constant.

In terms of β_n the length of the pile-up region in each scaling regime is given by $\ell_n^{(1)} = n^2\beta_n^2 h$, $\ell_n^{(2-4)} = n\beta_n h$ and $\ell_n^{(5)} \sim nh\log(\beta_n^2)$, respectively; clearly the length of the pile-up region increases when going from (1) to (5). We notice that the transition between $\ell_n^{(1)}$ and $\ell_n^{(2-4)}$ happens exactly in the first critical regime (case (2)), where $\beta_n \sim 1/n$. Concerning the transition between $\ell_n^{(2-4)}$ and $\ell_n^{(5)}$, although $\ell_n^{(5)} \le \ell_n^{(2-4)}$ always, $\ell_n^{(5)}$ is acceptable only when β_n is at least order one (since otherwise $\ell_n^{(5)} \le 0$, inadmissible). And this corresponds to the second critical regime (case (4)).

5.4. Mechanical interpretation of β_n.

The role of β_n and of the different asymptotic regimes can be understood as follows. Define the average dimensional distance between two walls (assuming n even) as

$$\Delta\tilde{x} := \frac{\tilde{x}_{n/2}}{n/2}. \tag{57}$$

Note that $\tilde{x}_{n/2}$ is a 'middle' wall, and therefore a reasonable indication of the size of the pileup. Assuming cases (2)–(4), where $\ell_n^{(2-4)} = n\beta_n h$, we can then rewrite (57) as

$$\frac{\Delta\tilde{x}}{h} = 2x_{n/2}\beta_n.$$

Since the non-dimensional positions are obtained by rescaling the positions $\tilde{x}$ by the pile-up length, it is natural to assume that $x_{n/2} \sim 1$. Hence the relation above indicates that β_n is a measure of the aspect ratio $\Delta\tilde{x}/h$, or, put differently, $n\beta_n$ is a measure of the total length of the pileup, relative to h.

Moreover, the dimensionless parameter β_n measures the elastic properties of the medium (described by K) in comparison with the strength of the pile-up driving force σ. Large β_n,

therefore, corresponds to weak forcing, and small β_n to strong forcing. Stronger forcing pushes the dislocation walls closer to each other; when $n\beta_n \to 0$, the forcing pushes the walls so close to each other that their distance is always smaller than h, so that V is only sampled close to the logarithmic singularity. Similarly, when $\beta_n \to \infty$, the forcing is so weak that the distance between the walls falls in the exponential tails of V. The intermediate regime is characterized by dislocation walls that span the range from 'smaller than h' to 'larger than h'.

We notice that one could use as alternative scaling parameter the non-dimensional stress $\hat{\sigma}_{\text{ext}} := \sigma h/K$ introduced in [18]. In terms of $\hat{\sigma}_{\text{ext}}$ the critical scalings would be $\hat{\sigma}_{\text{ext}} \sim n$ (corresponding to $n\beta_n \sim 1$) and $\hat{\sigma}_{\text{ext}} \sim 1/n$ (corresponding to $\beta_n \sim 1$). We believe, however, that the parameter β_n used in our analysis has a clearer geometric interpretation in terms of the local dislocation arrangements, which is one of the key points of the present paper.

5.5. More general dislocations arrangements and extensions.

A natural extension of this work is to apply our rigorous upscaling procedure to more general dislocation arrangements. A first direction is the study of *random walls*, namely perfectly straight (possibly finite) dislocation walls where the spacing between dislocations is not constant. As pointed out in [18] the problem in this more general case is genuinely two-dimensional, and hence much more difficult to treat. We refer also to [31] for a related discussion on random walls of dislocations.

Another possible direction of investigate is the boundary layers analysis. We notice from Figures 7, 8, 9, 12 and 13 that the agreement between the discrete and the continuum optimal densities fails close to the boundary, due to the presence of boundary layers. The reason for this is that the continuum upscaled energy is a *bulk* energy, while the boundary layers are, clearly, *boundary* effects. To capture the boundary layers one could try to consider a so-called "development" of the discrete energy by Γ-convergence as done for instance in [4] in the case of fracture.

Other possible approaches that could be used to describe boundary layers are presented in [20] and [30].

Acknowledgments

The research of L. Scardia was carried out under the project number M22.2.09342 in the framework of the Research Program of the Materials innovation institute (M2i) (www.m2i.nl).

The research of M. A. Peletier has received funding from the ITN "FIRST" of the Seventh Framework Programme of the European Community (grant agreement number 238702), and from the NWO Vernieuwingsimpuls (VICI scheme). The authors would like to thank Jan Zeman and Andrea Braides for their fruitful comments on the paper. Specifically, it was Jan Zeman who pointed us to the possibility of applying Γ-convergence to this setup.

[1] Alicandro R., Cicalese M. and Ponsiglione M.: Variational equivalence between Ginzburg-Landau, XY spin systems and screw dislocation energies. *Indiana Univ. Math. J.*. To appear.

[2] Baskaran R., Sreekanth A., Mesarovic S. and Zbib H.M.: Energies and distributions of dislocations in stacked pile-ups. *Int. J. Solids Struc.*, **47** (2010), 1144–1153.

[3] Bayley C.J., Brekelmans M.A.M. and Geers M.G.D.: A comparison of dislocation induced back stress formulations in strain gradient crystal plasticity. *Int. J. Solids Struct.*, **43** (2006), 7268–7286.

[4] Braides A. and Cicalese M.: Surface energies in nonconvex discrete systems. *Math. Models Methods Appl. Sci.*, **17** (2007), 985–1037.

[5] Braides A., Dal Maso G. and Garroni A.: Variational formulation of softening phenomena in fracture mechanics: the one-dimensional case. *Arch. Ration. Mech. Anal.*, **146** (1999), 23–58.

[6] Dal Maso G.: An Introduction to Γ-Convergence. Birkhäuser, 1993.
[7] Deng J. and El-Azab A.: Mathematical and computational modelling of correlations in dislocation dynamics. *Model. Simul. Mater. Sci. Eng.*, **17** (2009).
[8] El-Azab A.: Statistical mechanics treatment of the evolution of dislocation distributions in single crystals. *Phys. Rev. B*, **61**/18 (2000), 11956–11966.
[9] Eshelby J.D., Frank F.C. and Nabarro F.R.N.: The equilibrium of linear arrays of dislocations. *Philos. Mag.*, **43** (1951), 351–364.
[10] Evers L.P., Brekelmans W.A.M. and Geers M.G.D.: Scale dependent crystal plasticity framework with dislocation density and grain boundary effects. *Int. J. Solids Struc.*, **41** (2004) 5209–5230.
[11] Garroni A., Leoni G., Ponsiglione M.: Gradient theory for plasticity via homogenization of discrete dislocations. *J. Eur. Math. Soc.*, **12** (2010), 1231–1266.
[12] Garroni A., Müller S.: A variational model for dislocations in the line tension limit. *Arch. Ration. Mech. Anal.* **181** (2006), 535–578.
[13] Geers M.G.D., Peerlings R.H.J., Peletier M.A. and Scardia L.: Asymptotic behaviour of a pile-up of infinite walls of edge dislocations. *Arch. Ration. Mech. Anal.*, **209** (2013), 495–539.
[14] Geus, de T.W.J., Peerlings R.H.J. and Hirschberger C.B.: An analysis of the pile-up of infinite walls of edge dislocations. *Mech. Res. Commun.*, DOI: 10.1016/j.mechrescom.2013.08.010.
[15] Groma I.: Link between the microscopic and mesoscopic length-scale description of the collective behavior of dislocations. *Phys. Rev. B*, **56**/10 (1997), 5807–5813.
[16] Groma I., Csikor F.F. and Zaiser M.: Spatial correlation and higher-order gradient terms in a continuum description of dislocation dynamics. *Acta Mater.*, **51** (20030, 1271–1281.
[17] Gurtin M.E., Anand L. and Lele S.P.: Gradient single-crystal plasticity with free energy dependent on dislocation densities. *J. Mech. Phys. Solids*, **55** (2007), 1853–1878.
[18] Hall C.L.: Asymptotic analysis of a pile-up of edge dislocation walls. *Mat. Sci. Eng. A - Struct.*, **530** (2011), 144–148.
[19] Hall C.L.: Asymptotic expressions for the nearest and furthest dislocations in a pile-up against a grain boundary. *Philos. Mag.*, **90** (2010), 3879–3890.
[20] Hall C.L., Chapman S.J. and Ockendon J.R.: Asymptotic analysis of a system of equations arising in dislocation theory. *SIAM J. Appl. Math.*, 2010.
[21] Head A.K. and Louat N.: The distribution of dislocations in linear arrays. *Aust. J. Phys.*, **8**/1 (1955), 1–7.
[22] Hirth J.P. and Lothe J.: Theory of dislocations. John Wiley & Sons, 1982.
[23] Hull D. and Bacon D. J.: Introduction to dislocations. Butterworth-Heinemann, 2001.
[24] Mesarovic S., Baskaran R. and Panchenko A.: Thermodynamic coarsening of dislocation mechanics and the size-dependent continuum crystal plasticity. *J. Mech. Phys. Solids*, **58**/3 (2010), 311–329.
[25] Muschelišvili N. I. and Radok J. R. M.: Singular Integral Equations: Boundary Problems of Function Theory and Their Application to Mathematical Physics. Wolters-Noordhoff publishing, 1953.
[26] Ponsiglione M.: Elastic energy stored in a crystal induced by screw dislocations: From discrete to continuous. *SIAM J. Math. Anal.*, **39**/2 (2007), 449–469.
[27] Roy A. and Acharya A.: Size effects and idealized dislocation microstructure at small scales: prediction of a phenomenological model of Mesoscopic Field Dislocation Mechanics. Part II. *J. Mech. Phys. Solids*, **54**/8 (2006), 1711-1743.
[28] Roy A., Peerlings R.H.J., Geers M.G.D. and Kasyanyuk Y.: Continnum modeling of dislocation interactions: Why discreteness matters? *Mat. Sci. Eng. A - Struct.*, **486** (2008), 653–661.
[29] Schlömerkemper A. and Schmidt B.: Discrete-to-continuum limits of magnetic forces in dependence on the distance between bodies. *Arch. Rational Mech. Anal.* (2008).
[30] Voskoboinikov R.E., Chapman S.J., Ockendon, J.R. and Allwright D.J.: Continuum and discrete models of dislocation pile-ups. I. Pile-ups at a lock. *J. Mech. Phys. Solids*, **55** (2007), 2007–2025.
[31] Zaiser M. and Groma I.: Some limitations of dislocation walls as models for plastic boundary layers. *AIP Conference Proceedings*, **1389** (2011), 1540–1543.